Influence of Band-Gap Opening on Ballistic Electron Transport in Bilayer Graphene and Graphene Nanoribbon FETs

Sako, Ryutaro
Tsuchiya, Hideaki
Ogawa, Matsuto

Influence of Band-Gap Opening on Ballistic Electron Transport in Bilayer Graphene and Graphene Nanoribbon FETs

Ryūtaro Sako, Hideaki Tsuchiya, *Senior Member*, *IEEE*, and Matsuto Ogawa, *Senior Member*, *IEEE*

Department of Electrical and Electronic Engineering, Graduate School of Engineering, Kobe University
1-1, Rokko-dai, Nada-ku, Kobe 657-8501, Japan

Although graphene is a zero-gap semiconductor, band-gap energies up to several hundreds millielectron volts have been introduced by utilizing quantum mechanical confinement in nanoribbon structures or symmetry breaking between two carbon layers in bilayer graphenes. However, the opening of a band-gap causes a significant reduction in carrier velocity due to the modulation of bandstructures in their low energy spectrums. In this paper, we study intrinsic effects of the band-gap opening on ballistic electron transport in graphene nanoribbons (GNRs) and bilayer graphenes (BLGs) based on a computational approach, and discuss the ultimate device performances of field-effect transistors (FETs) with those semiconducting graphene channels. We have shown that an increase of external electric field in BLG-FET to obtain a larger band-gap energy substantially degrades its electrical characteristics because of de-acceleration of electrons due to a Mexican hat structure, and therefore GNR-FET outperforms in principle BLG-FET.

***Index Terms*—bilayer graphene, graphene nanoribbon, band-gap opening, Mexican hat structure, FET, ballistic transport**

I. Introduction

GRAPHENE-BASED devices are promising candidates to realize higher-speed operation of field-effect transistors (FETs), because a high carrier mobility of more than 10,000 $cm^2\ V^{-1}\ s^{-1}$ is experimentally obtained by using the simple mechanical exfoliation of bulk graphite [1], and even giant carrier mobility in excess of 200,000 $cm^2\ V^{-1}\ s^{-1}$ is reported by suspending single layer graphene to eliminate residual impurities on graphene surface [2]. However, on-off current ratio of graphene channel FETs is very small due to the lack of band-gap. Several methods have been proposed to open a band-gap, such as graphene nanoribbon (GNR) using quantum confinement effect in its transverse direction [3]-[7], and bilayer graphene (BLG) introducing symmetry breaking between two carbon layers via an external electric field [8]-[10] or interaction between a graphene layer and its substrate [11], [12]. Previous theoretical calculations have shown that armchair-edged GNRs (A-GNRs) exhibit larger band-gaps than those of BLGs applied by a vertical electric field, and more interestingly they have quite different dispersion relationship in their low-energy spectrums. For instance, in BLGs, a Mexican hat structure with a negative effective mass appears even under a relatively small vertical electric field [13]-[16]. On the other hand, A-GNRs still sustain a linear dispersion relationship until the obtained band-gap energy increases up to several hundred millielectron volts by decreasing the ribbon width [4], [7], [16]-[19]. Therefore, superior carrier transport in A-GNRs has been theoretically predicted [16].

As mentioned above, the electronic states of A-GNRs and BLGs highly depend on geometrical configurations and operating conditions, and thus systematic investigation is needed to understand their relative advantages for use in FET channels. However, only spot data have been used to assess their upper-limit performances so far, especially for BLG-FETs [15], [16]. With recent progress in atomically precise fabrication techniques both for GNR [20] and BLG [21], it becomes important to clarify intrinsic effects of the band-gap opening on electron transport in A-GNR-FETs and BLG-FETs. In this paper, we address the subject and systematically investigate the ultimate device performances of both FETs, based on a computational approach.

Manuscript received May 17, 2011

The authors are with the Department of Electrical and Electronic Engineering, Graduate School of Engineering, Kobe University, 1-1, Rokko-dai, Nada-ku, Kobe 657-8501, Japan (e-mail: 119t226t@stu.kobe-u.ac.jp, tsuchiya@eedept.kobe-u.ac.jp, ogawa@eedept.kobe-u.ac.jp). This work was supported by the Semiconductor Technology Academic Research Center (STARC).

II. Simulation Model

Fig. 1 shows (a) the atomic models for BLG and A-GNR, (b) the schematic diagram of the simulated BLG/A-GNR-FETs, and (c) self-consistent two-dimensional (2D) electrostatics used in a top-of-the-barrier (ToB) ballistic MOSFET model [22]. BLG consists of two A-B-stacked monolayers of graphene, while the edges of A-GNR are assumed to be terminated by hydrogen atoms. BLG is placed in vertical electric field F and A-GNR has the number of atoms in its transverse direction N and ribbon width W. As for the FET structure in Fig. 1 (b), the source and drain are assumed to be heavily doped BLG/A-GNR contacts with $N_D = 1\times10^{20}cm^{-3}$ and the channel is intrinsic. The gate insulator is assumed to be HfO_2 with a dielectric constant of 23.4 ε_0, which contributes to reduce the electric field impressed to the gate insulator. For BLG-FET, we assumed that the vertical electric field F is spatially constant throughout the device and is independent of both gate and drain voltages. This implies that F is solely induced by impurity concentration in the substrate. Therefore, charge density in the channel is controlled by the top gate electrostatics while maintaining a constant band-gap, which means that a gate voltage-induced band-gap modulation and screening of the vertical electric field by positive charges injected in the channel due to band-to-band tunneling [23], [24], and also effect of edge roughness [25] are ignored in this study. We consider that these

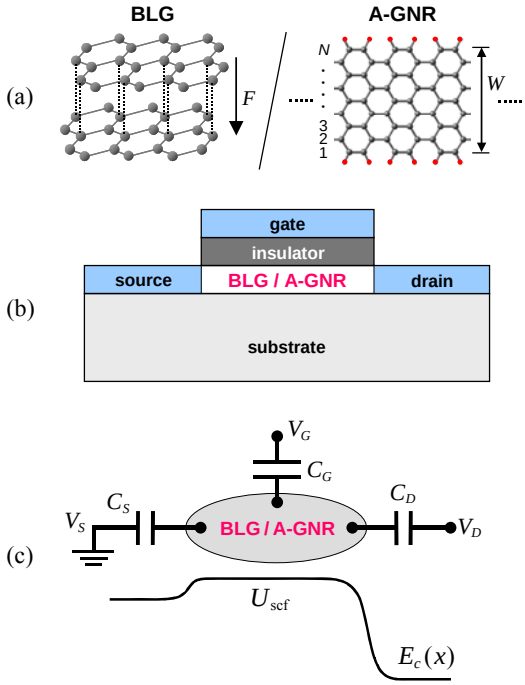

Fig. 1. (a) Atomic models for BLG and A-GNR, (b) schematic diagram of the simulated BLG/A-GNR-FETs, and (c) self-consistent 2D electrostatics used in top-of-the-barrier (ToB) ballistic MOSFET model. The edges of A-GNR are assumed to be terminated by hydrogen atoms. BLG is placed in vertical electric field F and A-GNR has the number of atoms in its transverse direction N and ribbon width W. As for the FET structure, the source and drain are assumed to be heavily doped BLG/A-GNR contacts while the channel is intrinsic. The gate insulator is assumed to be HfO_2 with a dielectric constant of 23.4 ε_0.

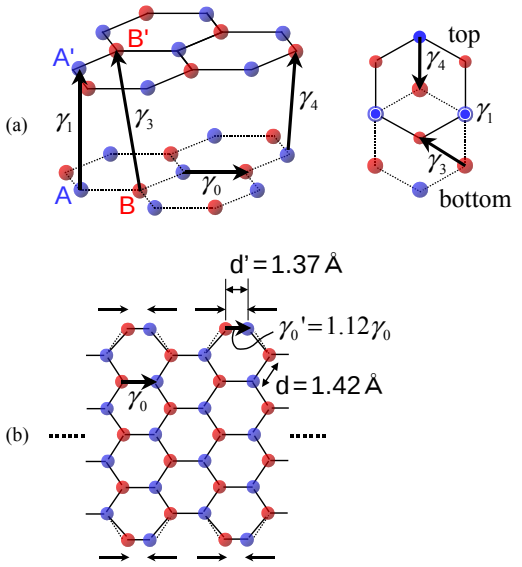

Fig. 2. Atomic structures of (a) BLG and (b) A-GNR, and various hopping parameters. The values of the hopping parameters are indicated in the text. In (b), the carbon-carbon bond lengths at the edges are shortened by about 3.5% as compared to other carbon-carbon bonds inside the ribbon.

simplifications are reasonable at least for ultimate performance estimation in the on-state. For A-GNR-FET, we adopted 1D perfect source and drain having the same width as the channel, since metal-induced-gap states are not produced in such 1D perfect contacts [26], [27]. In the ToB model, the difference in the number of graphene monolayers between BLG and A-GNR is taken into account in calculating the bandstructures and thus density-of-states for carriers, while spatial distributions of carriers and currents are not considered. In this paper, we assume that $C_G >> C_D$, C_S, which means that the gate has perfect electrostatic control over the channel. Though edge roughness scattering is extremely important to determine the electron mobility in long-channel A-GNR-FETs, its role in ultra-short channel devices is not well understood. Furthermore, graphene's mean free path is generally longer than the channel length used in this study. Therefore, we considered that scattering and static disorder have less impact on the band-gap opening and on the electron transport in the present ultra-short graphene channels, and neglected them.

Since the atomistic band structure of graphene channels has a crucial role in determining device performances of graphene-based FETs [15], [16], we computed the electronic bandstructures of BLG and A-GNR using a tight-binding (TB) approach with a p_z orbital basis set as shown in Fig. 2 [28]. One p_z orbital per atom is enough for atomistic physical description since s, p_x, and p_y are far from the Fermi level and do not play an important role for electron transport. The intralayer nearest-neighbor p_z orbital hopping amplitude γ_0 = 2.6 eV, the interlayer A-A' tunneling amplitude γ_1 = 0.34 eV, the interlayer B-B' coupling γ_3 = 0.3 eV and the interlayer A-B' coupling γ_4 = 0 eV are used [14]. Effect of the vertical electric field F in BLG is considered by increasing potential energy in the upper graphene layer by eFd, where d is the interlayer separation, that is, d = 0.335 nm. All carbon-carbon bond lengths are taken as 0.142 nm, but those at the edges of A-GNR are shortened to be 0.137 nm, as shown in Fig. 2 (b) [7], [17], [19]. This is because carbon-carbon bonds at the edges, which are also bonded to hydrogen atoms to terminate dangling bonds, are about 3.5 % shorter than other carbon-carbon bonds inside the ribbon, according to previous first-principles relaxation calculations [7]. Furthermore, to fit the first-principles bandstructure results, we used a different p_z orbital hopping amplitude of $\gamma_0' = 1.12\ \gamma_0$ for the edge bonds in A-GNR [7], [29]. As previously reported, the edge bond relaxation has a significant influence on the band-gap energy [7], [18], [19], and also on the carrier effective mass [19] of A-GNRs.

III. Band-Gap Energies

Although the band-gap opening in BLG and A-GNR has been already reported in other studies, we again present it in this section to clarify their potentials for the FET application, and exhibit basic data for further discussion regarding their electrical characteristics. Fig. 3 shows the computed band-gap energies of (a) BLG as a function of external electric field F_{ext} and (b) A-GNR as a function of ribbon width W. In Fig. 3 (a), we used an approximate relationship between the external electric field F_{ext} and the internal electric field F as in a form of $F \approx (1/3)\ F_{ext}$ [14], which is to consider the screening effect of the external interlayer potential due to the Hartree potential.

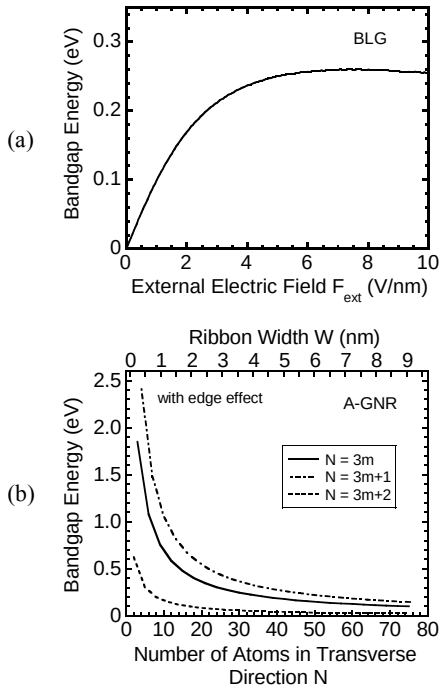

Fig. 3. Band-gap energies of (a) BLG as a function of external electric field F_{ext} and of (b) A-GNR as a function of ribbon width W. In (a), an approximate relationship between the external electric field F_{ext} and the internal electric field F as in a form of $F \approx (1/3)\, F_{ext}$ [14] was used, which is to consider the screening effect of the external interlayer potential due to the Hartree potential. In (b), m is a positive integer.

In Fig. 3 (b), we note that there are no metallic nanoribbons and the band-gaps are well separated into three different groups, depending on a positive integer of m [7], [18], [19]. Here, we can find a noticeable difference in band-gap energies between BLG and A-GNR. Specifically, the band-gap energy of BLG increases with F_{ext}, but saturates at around 0.25 ~ 0.26 eV beyond F_{ext} = 5 V/nm. On the other hand, the band-gap energy of A-GNR continues to increase as the ribbon width decreases, for example, a few electron volts is achievable for less than 1 nm ribbon width. This is obviously due to the quantum confinement effect. The above results mean that A-GNR has the capability opening larger band-gaps than BLG. However, their dispersion relationship in low-energy regime, which basically governs device performance of FETs, is known to drastically change with the band-gap opening [4], [7], [14]-[19]. So, in terms of the FET application, a comparison of transport properties under the same band-gap energy becomes important. In the following sections, we will discuss this point by comparing electrical characteristics of BLG-FETs and A-GNR-FETs considering their atomistic bandstructures. In this regard, we focus on A-GNR-FETs with $N = 3m$ group, since they are expected to provide superior device performance over $N = 3m + 1$ and $3m + 2$ groups [19].

IV. Small Band-Gap Regime

In this section, we discuss the electrical characteristics under a relatively small band-gap energy, but being sufficiently larger than the thermal energy at room

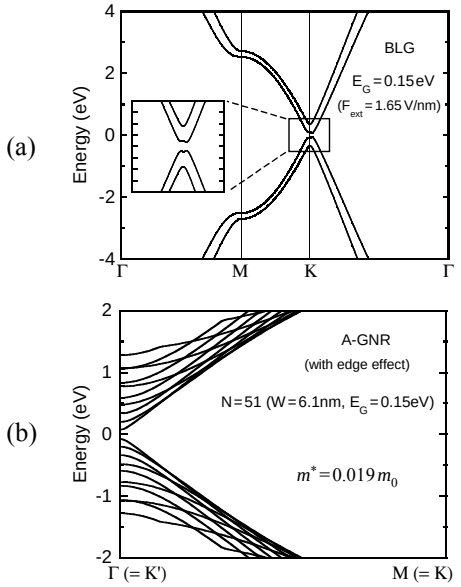

Fig. 4. Bandstructures computed for (a) BLG under F_{ext} = 1.65 V/nm and (b) A-GNR with W = 6.1 nm, both of which have a band-gap energy of E_G = 0.15 eV. As shown in the inset of (a), a Mexican hat structure with a negative effective mass appears in the BLG at the K point (Dirac point).

temperature. First, Fig. 4 shows the bandstructures computed for (a) the BLG under F_{ext} = 1.65 V/nm and (b) the A-GNR with W = 6.1 nm, both of which have a band-gap energy of E_G = 0.15 eV. As shown in the inset of Fig. 4 (a), a Mexican hat structure with a negative effective mass appears in the BLG at the K point (Dirac point). On the other hand, a linear dispersion relationship is still observed in the A-GNR of Fig. 4 (b) where its electron effective mass is estimated to be 0.019 m_0, despite the opening of a finite band-gap.

Now, we evaluate the ultimate device performances when the BLG and A-GNR are applied to the FET channels as shown in Fig. 1 (b). In this study, to directly examine the influences of atomistic bandstructures, we used the ToB ballistic MOSFET model [22], as schematically shown in Fig. 1 (c). The model has been proven to be suitable for a systematic study comparing the performance limits of atomistic transistors including III-V nanowire [30] and carbon-based FETs [16], [19], [31]-[33]. Fig. 5 shows comparisons in the drain current versus gate voltage (I_D - V_G) characteristics and in the averaged electron velocities and the transit times computed for the BLG- and A-GNR-FETs with gate oxide thickness of (a) T_{ox} = 9 nm (EOT = 1.5 nm) and (b) 3 nm (EOT = 0.5 nm), where the gate oxide was assumed to be HfO_2. In the calculation of the transit times, the channel length is assumed to be 10 nm. Here, the current drive is expressed in units of drain current per unit width even for A-GNR-FET, which will be suited to represent the current drive of closely spaced nanoribbon arrays such as nanomesh [34]. Since the channel length is set as 10 nm and the high-k gate oxide is employed, we can expect excellent electrostatic control to prevent source-drain direct tunneling. Furthermore, the drain voltage is set sufficiently small (V_D = 0.3 V), and we also ignored band-to-band tunneling in this study. For T_{ox} = 9 nm, the A-GNR-FET provides not only larger drain current,

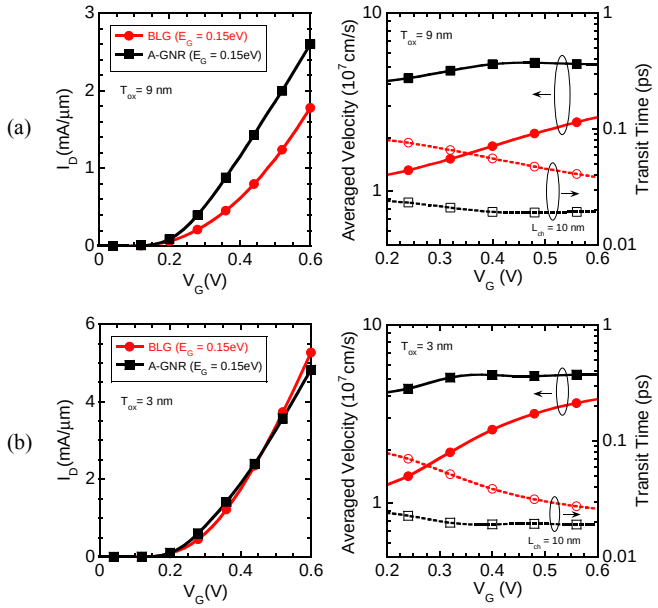

Fig. 5. Comparisons in I_D - V_G characteristics and in averaged electron velocities and transit times computed for BLG- and A-GNR-FETs with E_G = 0.15 eV for (a) T_{ox} = 9 nm (EOT = 1.5 nm) and (b) 3 nm (EOT = 0.5 nm), where the gate oxide was assumed to be HfO_2. In the right column figures, ■ and □ represent A-GNR, and ● and ○ BLG. The current density at V_G = 0 V is set as 0.06 μA/μm, and channel length is assumed to be 10 nm in the calculation of transit times. V_D is set at 0.3 V and temperature is 300 K.

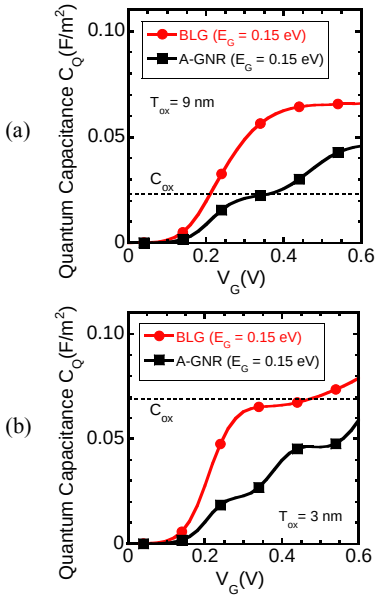

Fig. 6. Comparisons in quantum capacitances computed for BLG- and A-GNR-FETs with E_G = 0.15 eV, where (a) T_{ox} = 9 nm and (b) 3 nm. The horizontal dashed lines represent the oxide capacitances determined by $C_{ox} = \varepsilon_{ox} / T_{ox}$.

but also higher averaged velocity than the BLG-FET. This is the anticipated result, considering the difference between their dispersion relationships in the low energy regime as shown in Fig. 4.

Here, we should point out that the averaged electron velocity of the A-GNR-FET is nearly independent of the gate bias voltage, since the A-GNR channel has an almost linear dispersion relationship as shown in Fig. 4 (b). In other words, at the on-state the Fermi level is deep inside the conduction band and higher subbands get populated. Though carriers in the higher subbands transport under the influence of a partly parabolic dispersion relationship, a large part of carriers are still distributed into a linear part of the dispersion curves. Therefore, the average electron velocity hardly changes even if the gate bias increases. For the same reason, the averaged electron velocities are almost independent of the gate oxide thickness in the A-GNR-FET. On the other hand, in the BLG-FET with smaller T_{ox}, a number of electrons increasingly occupy a higher-momentum region, which has linear dispersion relationship even in BLGs. Therefore, as shown in Fig. 5 (b) the average electron velocity increases to improve the I_D - V_G characteristics and the transit times of the BLG-FET by decreasing T_{ox}.

It is also noteworthy that for T_{ox} = 3 nm in Fig. 5 (b), the current drive of A-GNR-FET is almost identical to that of BLG-FET, even though the carrier velocity, which is proportional to the reciprocal of device delay, is undoubtedly higher than the BLG-FET. This is due to the reduction in the total gate capacitance influenced by the quantum capacitance of the channels, particularly, in the A-GNR-FET. Since the quantum capacitance is determined by the density of states for carriers, A-GNR-FET with a smaller effective mass is more likely to be affected by the quantum capacitance under such a very small T_{ox}. We actually computed the quantum capacitances for both FETs by using the ToB model and compare them as shown in Fig. 6, where (a) T_{ox} = 9 nm and (b) 3 nm. The horizontal dashed lines represent the oxide capacitances determined by $C_{ox} = \varepsilon_{ox} / T_{ox}$. The quantum capacitance is numerically calculated from $C_Q = \partial(qN) / \partial(-U_{scf} / q)$, where qN and U_{scf} are the charge density and the potential at the top of the barrier, respectively [22], [30]. It is found that the C_Q in A-GNR-FET is remarkably smaller than the C_{ox} when T_{ox} is 3 nm. On the other hand, the C_Q in BLG-FET is still comparable to the C_{ox} at the on state for T_{ox} = 3 nm, because the Mexican hat structure provides larger density of states than those in A-GNR. Consequently, the current drive of A-GNR-FET degrades considerably due to the quantum capacitance under such a very small T_{ox}, as shown in Fig. 5 (b).

V. Large Band-Gap Regime

Next, we study the performances under a larger band-gap energy, that is, close to the maximum band-gap energy in BLG. Fig. 7 shows the bandstructures computed for the (a) BLG under F_{ext} = 5.0 V/nm and (b) A-GNR with W = 3.6 nm, both of which have a band-gap energy of E_G = 0.25 eV. In Fig. 7 (a), the result computed for F_{ext} = 8.0 V/nm is also plotted for further discussion, where the band-gap energy only slightly increases to E_G = 0.26 eV, but its dispersion relationship drastically changes as shown in the inset. Namely, the Mexican hat structure becomes more warped by increasing the external electric field, even though the opened band-gap energy is almost the same. So, de-acceleration of electrons due to the negative effective mass becomes more serious and probably causes further performance degradation. Such

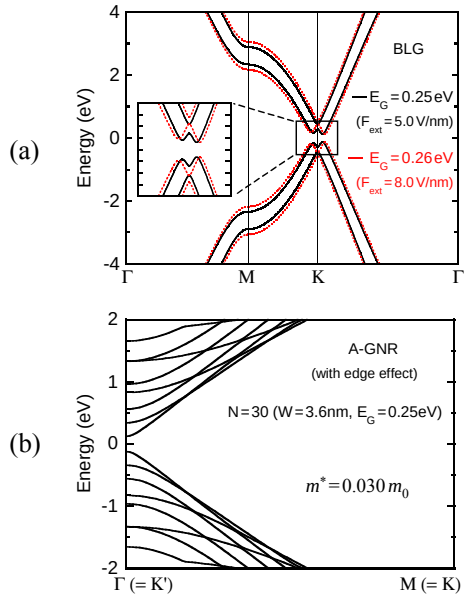

Fig. 7. Bandstructures computed for (a) BLG under F_{ext} = 5.0 V/nm and (b) A-GNR with W = 3.6 nm, both of which have a band-gap energy of E_G = 0.25 eV. In (a), the result computed for F_{ext} = 8.0 V/nm is also plotted, where the band-gap energy only slightly increases to E_G = 0.26 eV, while its dispersion relationship drastically changes as shown in the inset.

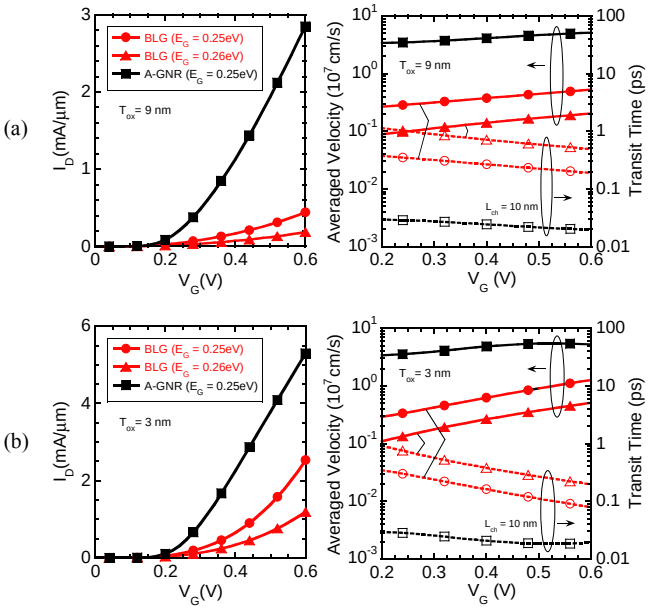

Fig. 8. Comparisons in I_D - V_G characteristics and in averaged electron velocities and transit times computed for BLG- and A-GNR-FETs with E_G = 0.25 eV. For BLG-FET, the results computed for F_{ext} = 8.0 V/nm, providing E_G = 0.26 eV, are also plotted. The gate oxide thickness is taken as (a) T_{ox} = 9 nm and (b) 3 nm, where the gate oxide was assumed to be HfO_2. In the right column figures, ■ and □ represent A-GNR, and ●, ▲, ○ and Δ BLGs. The calculation conditions were the same as in Fig. 5.

consideration is actually confirmed by simulating the electrical characteristics as shown in Fig. 8, where the calculation conditions were the same as in Fig. 5. For both of T_{ox} = 9 nm and 3 nm, the BLG-FETs exhibit much inferior performances compared to the A-GNR-FET. In particular, the increasing F_{ext} substantially degrades the electrical characteristics of BLG-FETs, as expected above. This also means that the device performance of BLG-FETs can significantly differ even if they have nearly equal band-gap energies.

In addition, it is found that the characteristics of the A-GNR-FET are almost unchanged by increasing the band-gap energy from 0.15 eV (Fig. 5) to 0.25 eV (Fig. 8), since the effective mass only slightly increases to 0.030 m_0. This behavior is in contrast to that of BLG-FETs. However, as reported in [16], A-GNR-FETs with larger band-gap energy than ~ 0.4 eV exhibit marked degradation of the device performances, since a parabolic dispersion relationship with a heavier effective mass appears in A-GNRs. Consequently, there should be a trade-off relationship between band-gap energy and carrier velocity in A-GNR-FETs as well as in BLG-FETs. Nonetheless, the present results suggest that ideal A-GNR-FETs outperform in principle BLG-FETs consisting of the multilayer graphene architecture [35].

VI. Conclusion

To clarify intrinsic effects of the band-gap opening on electron transport in A-GNR-FETs and BLG-FETs, we have systematically investigated their upper-limit performances based on TB bandstructure calculation and ballistic MOSFET model. We have found that the increase of external electric field in BLG-FET to obtain a larger band-gap energy significantly degrades the electrical characteristics, because a Mexican hat structure becomes more warped and de-acceleration of electrons due to a negative effective mass causes a serious performance degradation. Therefore, in principle A-GNR-FETs outperform BLG-FETs. However, we have also pointed out that there is a trade-off relationship between band-gap energy and carrier velocity in applying such semiconducting graphene channels into high-speed logic circuits.

References

[1] K.S. Novoselov, A.K. Geim, S.V. Morozov, D. Jiang, Y. Zhang, S.V. Dubonos, I.V. Grigorieva, and A.A. Firsov, "Electric field effect in atomically thin carbon films," *Science*, vol. 306, pp. 666-669, Oct. 2004.

[2] K.I. Bolotin, K.J. Sikes, Z. Jiang, M. Klima, G. Fudenberg, J. Hone, P. Kim, and H.L. Stormer, "Ultrahigh electron mobility in suspended graphene," *Solid State Comm.*, vol. 146, pp. 351-355, 2008.

[3] M. Fujita, K. Wakabayashi, K. Nakada, and K. Kusakabe, "Peculiar localized state at zigzag graphite edge," *J. Phys. Soc. Jpn.*, vol. 65, no. 7, pp. 1920-1923, Jul. 1996.

[4] G. Liang, N. Neophytou, D.E. Nikonov, and M.S. Lundstrom, "Performance projections for ballistic graphene nanoribbon field-effect transistors," *IEEE Trans. on Electron Devices*, vol. 54, no. 4, pp. 677-682, Apr. 2007.

[5] M.Y. Han, B. Özyilmaz, Y. Zhang, and P. Kim, "Energy band-gap engineering of graphene nanoribbons," *Phys. Rev. Lett.*, vol. 98, no. 20, p. 206805, May 2007.

[6] X. Li, X. Wang, L. Zhang, S. Lee, and H. Dai, "Chemically derived, ultrasmooth graphene nanoribbon semiconductors," *Science*, vol. 319, pp. 1229-1232, Feb. 2008.

[7] Y.W. Son, M.L. Cohen, and S.G. Louie, "Energy gaps in graphene nanoribbons," *Phys. Rev. Lett.*, vol. 97, no. 21, p. 216803, Nov. 2006.

[8] T. Ohta, A. Bostwick, T. Seyller, K. Horn, and E. Rotenberg, "Controlling the electronic structure of bilayer graphene," *Science*, vol. 313, pp. 951-954, Aug. 2006.

[9] J. B. Oostinga, H. B. Heersche, X. Liu, A. F. Morpurgo, and L. M. K. Vandersypen, "Gate-induced insulating state in bilayer graphene devices," *Nature Materials*, vol. 7, pp. 151-157, Feb. 2008.

[10] Y. Zhang, T.-T. Tang, C. Girit, Z. Hao, M. C. Martin, A. Zettl, M. F. Crommie, Y. R. Shen, and F. Wang, "Direct observation of a widely tunable bandgap in bilayer graphene," *Nature*, vol. 459, pp. 820-823, June 2009.
[11] S. Zhou, G.-H. Gweon, A. Fedorov, P. First, W. de Heer, D.-H. Lee, F. Guinea, A. Castro Neto, and A. Lanzara, "Substrate-induced bandgap opening in epitaxial graphene," *Nature Materials*, vol. 6, pp. 770-775, Oct. 2007.
[12] G. Giovannetti, P. Khomyakov, G. Brockes, P. Kelly, and J. van den Brink, "Substrate-induced band gap in graphene on hexagonal boron nitride: *Ab initio* density functional calculations," *Phys. Rev. B*, vol. 76, p. 073103, Aug. 2007.
[13] E. McCann, "Asymmetry gap in the electronic band structure of bilayer graphene," *Phys. Rev. B*, vol. 74, p. 161403(R), Oct. 2006.
[14] H. Min, B. Sahu, S.K. Banerjee, and A.H. MacDonald, "*Ab initio* theory of gate induced gaps in graphene bilayers," *Phys. Rev. B*, vol. 75, no. 15, p. 155115, Apr. 2007.
[15] N. Harada, M. Ohfuti, and Y. Awano, "Performance estimation of graphene field-effect transistors using semiclassical Monte Carlo simulation," *Appl. Phys. Express*, vol. 1, p. 024002, Feb. 2008.
[16] H. Hosokawa, R. Sako, H. Ando, and H. Tsuchiya, "Performance comparisons of bilayer graphene and graphene nanoribbon field-effect transistors under ballistic transport," *Jpn. J. Appl. Phys.*, vol. 49, p. 110207, Nov. 2010.
[17] D. Gunlycke and C.T. White, "Tight-binding energy dispersions of armchair-edge graphene nanostrips," *Phys. Rev. B*, vol. 77, no. 11, p. 115116, Mar. 2008.
[18] H. Raza and E. C. Kan, "Armchair graphene nanoribbons: Electronic structure and electric-field modulation," *Phys. Rev. B*, vol. 77, p. 245434, June 2008.
[19] R. Sako, H. Hosokawa, and H. Tsuchiya, "Computational study on edge configuration and quantum confinement effects on graphene nanoribbon transport," *IEEE Electron Device Letters*, vol. 32, no. 1, pp. 6-8, Jan. 2011.
[20] J. Cai, P. Ruffieux, R. Jaafar, M. Bieri, T. Braun, S. Blankenburg, M. Muoth, A. P. Seitsonen, M. Saleh, X. Feng, K. Müllen, and R. Fasel, "Atomically precise bottom-up fabrication of graphene nanoribbons," *Nature*, vol. 466, pp. 470-473, July 2010.
[21] H. Miyazaki, K. Tsukagoshi, A. Kanda, M. Otani, and S. Okada, "Influence of disorder on conductance in bilayer graphene under perpendicular electric field," *Nano Lett.*, vol. 10, pp. 3888-3892, 2010.
[22] A. Rahman, J. Guo, S. Datta, and M.S. Lundstrom, "Theory of ballistic nanotransistors," *IEEE Trans. on Electron Devices*, vol. 50, no. 9, pp. 1853-1864, Sep. 2003.
[23] E. V. Castro, K. S. Novoselov, S. V. Morozov, N.M.R. Peres, J.M.B. Lopes dos Santos, J. Nilsson, F. Guinea, A. K. Geim, and A. H. Castro Neto, "Biased bilayer graphene: Semiconductor with a gap tunable by the electric field effect," *Phys. Rev. Lett.*, vol. 99, p. 216802, Nov. 2007.
[24] G. Fiori and G. Iannaccone, "On the possibility of tunable-gap bilayer graphene FET," *IEEE Electron Device Letters*, vol. 30, no. 3, pp. 261-264, Mar. 2009.
[25] D. Basu, M. J. Gilbert, L. F. Register, and S. K. Banerjee, "Effect of edge roughness on electronic transport in graphene nanoribbon channel metal-oxide-semiconductor field-effect transistors," *Appl. Phys. Lett.*, vol. 92, 042114, 2008.
[26] G. Liang, N. Neophytou, M. S. Lundstrom, and D. E. Nikonov, "Ballistic graphene nanoribbon metal-oxide-semiconductor field-effect transistors: A full real-space quantum transport simulation," *J. Appl. Phys.*, vol. 102, p. 054307, Sep. 2007.
[27] G. Liang, N. Neophytou, M. S. Lundstrom, and D. E. Nikonov, "Contact effects in graphene nanoribbon transistors," *Nano Lett.*, vol. 8, no. 7, pp. 1819-1824, 2008.
[28] A. H. Castro Neto, F. Guinea, N. M. R. Peres, K. S. Novoselov, and A. K. Geim, "The electronic properties of graphene," *Rev. Mod. Phys*, vol. 81, no. 1, pp. 109-162, Jan.-Mar. 2009.
[29] P. Zhao, J. Chauhan, and J. Guo, "Computational study of tunneling transistor based on graphene nanoribbon," *Nano Lett.*, vol. 9, no. 2, pp. 684-688, 2009.
[30] K. Alam and R. N. Sajjad, "Electronic properties and orientation-dependent performance of InAs nanowire transistors," *IEEE Trans. on Electron Devices*, vol. 57, no. 11, pp. 2880-2885, Nov. 2010.
[31] Y. Ouyang, Y. Yoon, and J. Guo, "Edge chemistry engineering of graphene nanoribbon transistors: A computational study," in *IEDM Tech. Dig.*, 2008, pp. 517-520.
[32] Y. Ouyang, Y. Yoon, J. K. Fodor, and J. Guo, "Comparison of performance limits for carbon nanoribbon and carbon nanotube transistors," *Appl. Phys. Lett.*, vol. 89, no. 20, 203107, 2006.
[33] H. Tsuchiya, H. Ando, S. Sawamoto, T. Maegawa, T. Hara, H. Yao, and M. Ogawa, "Comparisons of performance potentials of silicon nanowire and graphene nanoribbon MOSFETs considering first-principles bandstructure effects," *IEEE Trans. on Electron Devices*, vol. 57, no. 2, pp. 406-414, Feb. 2010.
[34] J. Bai, X. Zhong, S. Jiang, Y. Huang, and X. Duan, "Graphene nanomesh," *Nature Nanotech.*, vol. 5, pp. 190-194, Mar. 2010.
[35] K. Nagashio, T. Nishimura, K. Kita, and A. Toriumi, "Systematic investigation of the intrinsic channel properties and contact resistance of monolayer and multilayer graphene field-effect transistor," *Jpn. J. Appl. Phys.*, vol. 49, p. 051304, May 2010.

Ryūtaro Sako was born in Hyogo, Japan, on November 15, 1988. He received the B. S. degree in electrical and electronics engineering from Kobe University, Kobe, Japan, in 2011, and is currently working toward the M. S. degree at Kobe University. His research interests involve atomistic simulation of graphene nanotransistors.

Hideaki Tsuchiya (M'93–SM'01) received the B. S., M. S., and Ph. D. degrees all in electronic engineering from Kobe University, Kobe, Japan, in 1987, 1989, and 1993, respectively.

In 1993, he was with the Department of Electrical and Electronics Engineering, Kobe University, as a Research Associate. He has been engaged in research of quantum transport simulation of mesoscopic devices. From 1999 to 2000, he was a Visiting Scientist with the University of Illinois at Urbana-Champaign, IL, USA. Since 2003, he has been an Associate Professor with the Graduate School of Engineering, Kobe University. His current research includes the quantum transport modeling of nanoscale MOSFETs and the first principles simulation of atomic-scale devices.

Dr. Tsuchiya is a member of the Institute of Electronics, Information and Communication Engineers of Japan, and the Japan Society of Applied Physics. He received a Young Scientist Award in 1998 from the Japan Society of Applied Physics and an Outstanding Achievement Award for a pioneering research on nanoscale device simulator in 2006 from the Institute of Electronics, Information and Communication Engineers of Japan.

Matsuto Ogawa (M'85–SM'09) received the B.E. in electrical engineering from the University of Tokyo, Tokyo, Japan, in 1980, and the M.S. and Ph.D degrees in electronic engineering from the University of Tokyo, Tokyo, Japan, 1n 1982, and 1985, respectively.

In that year he became a research associate in the Department of Electronic Engineering, Kobe University, Kobe, Japan, where he is presently a Full Professor. He has been engaged in research of lightwave electronics and nano-scaled devices. His current research includes quantum transport modeling in nanostructures. From 1992 to the end of 1993, he was on leave at IBM T.J. Watson Research Center, NY, as a Visiting Scientist.

Dr. Ogawa is a member of the IEEE, the Japan Society of Applied Physics and the Institute of Electronics, Information and Communication Engineers (IEICE) of Japan. He received Electronics Society Award in 2006 from the IEICE and Project Research Award from the Semiconductor Technology Academic Research Center (STARC) in 2008.